Dalton Transactions

ROYAL SOCIETY OF CHEMISTRY

PERSPECTIVE

View Article Online
View Journal | View Issue

Cite this: *Dalton Trans.*, 2021, **50**, 6373

Liquid atomic layer deposition as emergent technology for the fabrication of thin films

Octavio Graniel, *[a] Josep Puigmartí-Luis *[b,c] and David Muñoz-Rojas *[a]

Received 22nd January 2021,
Accepted 9th March 2021

DOI: 10.1039/d1dt00232e

rsc.li/dalton

Atomic layer deposition (ALD) is widely recognized as a unique chemical vapor deposition technique for the fabrication of thin films with high conformality and precise thickness control down to the Ångstrom level, thereby allowing surface and interface nanoengineering. However, several challenges such as the availability of chemical precursors for ALD and the use of vacuum conditions have hampered its widespread adoption and scalability for mass production. In recent years, the liquid phase homolog of ALD, liquid atomic layer deposition (LALD), has emerged as a much simpler and versatile strategy to overcome some of the current constraints of ALD. This perspective describes the different strategies that have been explored to achieve conformality and sub-nanometer thickness control with LALD, as well as the current challenges it faces to become a part of the thin-film community toolbox, in particular its automation and compatibility with different types of substrates. In this regard, the important role of LALD as complementary technology to ALD is emphasized by comparing the different pathways to deposit the same material and the precursors used to do so.

Introduction

The preparation of thin films to improve the physical and chemical properties of materials is a widespread practice that has revolutionized the world since ancient times.[1] Thin films can be found in solar cells as transparent conductive oxide and absorber layers,[2] in aircraft components as corrosion-resistant layers,[3] in smart windows as thermochromic layers,[4] in arthroscopic microsurgery devices as optical layers,[5] and in data storage media (*e.g.* hard drives) as multilayer structures.[6] Interestingly, the development and improvement of thin film deposition technologies has coincided with the boom of the electronics industry.[7] Over the years, the scaling down of electronic components and, particularly, the broadening of industrial applications of artificial materials has demanded techniques that allow the fabrication of thin films with specific mechanical, chemical, optical, and electrical properties while precisely controlling their thickness and homogeneity.[8] For this reason, numerous methods have been developed to deposit thin films from both liquid and gas phases. In a recent review, a historical examination covering the evolution of thin film deposition technologies evidences the complementary progress that liquid-phase (*e.g.* electrodeposition, sol–gel processing) and gas-phase (*e.g.* sputtering, thermal evaporation) techniques have brought to the implementation of thin films in industrial processes.[9] In this context, it is worth mentioning that depending on the final application, the choice of thin film deposition technique is based on parameters such as the type of substrate to be coated, the material to be deposited, and the degree of conformality and step coverage. Moreover, when taking into account the economic factors, the use of approaches that involve high temperatures and vacuum conditions increases the fabrication costs of the final device or application and, therefore, should be taken into account when choosing a thin film deposition technique.[10]

Generally speaking, thin films can be produced from the gas phase by physical or chemical means.[11] Physical vapor deposition (PVD) encompasses techniques such as sputtering, arc vapor deposition, and thermal evaporation, while chemical techniques can be divided into chemical vapor deposition (CVD) and atomic layer deposition (ALD). It is worth noting that although physical and chemical processes rely on the efficient transport of materials in the gas phase to a solid substrate, in the chemical ones the film is formed from the product of a chemical reaction that involves one or more species. Bearing this in mind, ALD can be distinguished from PVD and CVD, both considered steady state techniques, because it is based on self-limiting chemical reactions that take place between the chemical species and the surface of the substrate to be coated.[12,13] Correspondingly, by exposing the substrate to alternate pulses of two or more different precursors, with a purging step in between, it is possible to precisely

[a]*Univ. Grenoble Alpes, CNRS, Grenoble INP, LMGP, 38000 Grenoble, France*
[b]*Departament de Ciència dels Materials i Química Física, Institut de Química Teòrica i Computacional, 08028 Barcelona, Spain*
[c]*ICREA, Catalan Institution for Research and Advanced Studies, Pg. Lluís Companys 23, 08010 Barcelona, Spain*

control the thickness of the film to be deposited down to a monolayer.[14,15] In addition, the conformality and uniformity of the films over three dimensional (3D) and high aspect ratio structures, coupled with the high scalability of the process (*e.g.*, spatial ALD [SALD]) and the diverse list of materials that can be prepared (*e.g.*, oxides, nitrides, sulfides, and metals), has made ALD an attractive technique for nanoscience and semiconductor technology.[16] However, ALD faces some drawbacks that have hampered its broader commercial and industrial adoption. For instance, the choice of chemical precursors for ALD, and therefore the range of materials that can be deposited, yet growing, is still limited: precursors need to be highly reactive while being robust enough to avoid thermal decomposition.[17,18] Moreover, the majority of ALD processes require vacuum conditions that are cumbersome for upscaling and increase operational costs.[19] Recently, several research groups have translated the main advantages of ALD (*i.e.* self-limiting behavior, conformality, and superior thickness control) to more gentle deposition methods in the liquid phase. The readily available solution chemistry knowledge, the less expensive equipment required to handle liquids rather than gases, and the possibility to deposit thin films at room temperature and pressure are some of the desirable characteristics that liquid phase ALD (LALD) has brought to the thin film community.

Here, we present a perspective report of the LALD literature. As a starting point, we briefly discuss some of the thin film deposition techniques that gave origin to LALD with a focus on the different names that the technique has received over time. Subsequently, we examine the gradual translation of ALD from the gas phase to the liquid phase by discussing several examples of LALD and the different molecular interactions driving the film growth. Finally, we identify the challenges relating to LALD development including the control of thin film properties and upscaling of the technology.

LALD historical background

The deposition of thin films from the liquid phase can be traced back as far as the 1800s when electrodeposition, sol–gel processing, and chemical bath deposition ([CBD], also known as chemical solution deposition [CSD]), were first explored.[9,20] However, it was not until 1985 that a technique based on sequential heterogeneous reactions was developed by Nicolau.[21] In contrast to CBD in which all the chemical species needed to deposit a thin film are simultaneously present in a reaction vessel, in the successive ionic layer adsorption and reaction (SILAR), the reactions are separated by an intermediate rinsing step with a pure solvent that avoids the formation of homogeneous precipitation in the solution.[22,23] The thin film growth cycle in SILAR can be described in four different steps (Fig. 1). The first step involves the immersion of a substrate into a cation solution and the formation of an electrical double layer by the adsorption of the cations on the negatively charged surface of the substrate. In

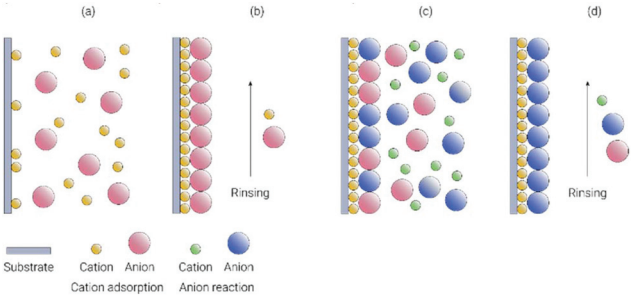

Fig. 1 Schematic representation of one SILAR cycle. (a) Cation adsorption, (b) rinsing to remove non-adsorbed ions, (c) anion reaction, and (d) rinsing to remove non-adsorbed ions. Adapted with permission from ref. 32. Copyright 2009, John Wiley & Sons.

the next step, the substrate is rinsed with a pure solvent to remove the excess adsorbed ions on the diffusion layer and leave only the tightly-bound inner layer. In the following step, the substrate is immersed in an anion solution and the anions from the solution diffuse toward the solid–solution interface and react to form a solid compound. In the final step, the substrate is rinsed with a pure solvent to remove unreacted ions from the diffusion layer and leave a surface to start a new cycle.

Since its conception, SILAR has been a key technique for the synthesis of metal chalcogenides and metal oxide thin films for applications in solar cells,[24,25] supercapacitors,[26,27] hydrogen production,[28,29] and biosensors.[30,31] Interestingly, Nicolau made a brief mention of the parallelism between SILAR and ALD (previously known as atomic layer epitaxy [ALE]) but did not make a thorough comparison of both techniques. It was not until 1995 that Lindroos *et al.* reintroduced SILAR under the name of liquid phase atomic layer epitaxy (LPALE) that a more detailed likeness between the techniques was established. In their work, they deposited ZnS thin films and pointed out some of the advantages and disadvantages of the technique. The low cost of the equipment and the low temperatures needed to grow thin films, coupled with the possibility of using thermally unstable precursors not available in gas phase ALD, are some of the main advantages of SILAR. On the other hand, although comparable in growth per cycle (1–3 Å), SILAR is slower than gas phase ALD due to the long time needed for the rinsing step, an action required to remove the excess adsorbed ions from the diffusion layer. In addition, the incompatibility of substrates (*e.g.* Si, Al_2O_3) with the frequently alkaline conditions and the need for excessive amounts of precursors and pure solvent also represents a constraint.

Following the same sequential and self-limiting behavior of ALD, in 1991, Gregory *et al.* developed the electrochemical atomic layer epitaxy (ECALE) or E-ALD as it is currently known.[33] E-ALD is based on the underpotential deposition (UPD) of an element onto another in a layer-by-layer fashion. As the electrochemical reactions taking place in E-ALD are performed within the UPD range, bulk deposition and island-

growth of the material are avoided owing to the more favorable deposition on the underlying substrate.[34] Although occurring in the condensed phase and at low temperatures, E-ALD falls outside the scope of this progress report as the majority of techniques that will be discussed here do not require an applied potential to deposit thin films. However, a more specialized and comprehensive bibliography is suggested for readers interested in the subject.[32,35,36]

In pursuit of a more controlled sol–gel process to deposit thin films, in 1996 Ichinose *et al.* introduced a surface sol–gel (SSG) iterative approach based on sequential condensation and hydrolysis reactions with intermediate rinsing and drying steps for the preparation of TiO_2, ZrO_2, and Al_2O_3 thin films.[37] By following the stepwise adsorption of the metal oxide precursors and their subsequent hydrolysis with a quartz crystal microbalance (QCM), a linear behavior of the film growth rate was demonstrated. Still, while the authors did not explicitly compare the SSG approach to ALD or SILAR, the striking resemblance between the techniques became evident afterwards.[38]

As stated above, the chemical interactions driving the growth of thin films in LALD are quite diverse (*e.g.* sol–gel, hydrolysis, redox reactions, polymerization) and each one of them has been explored independently over the years. For this reason, a general consensus has not been reached in the research community on whether the approaches discussed so far could be considered a part of a single technique (*i.e.* LALD). Therefore, although being referred to with different names, all the works that we will describe in the next section are considered as different variations of LALD.

Different approaches to achieve LALD

The ability to carefully control the growth of metal oxide thin films *via* stepwise sol–gel reactions of alkoxides represented a landmark in thin-film science. Certainly, the conventional methods used up to that point for depositing thin films by sol–gel processes (*e.g.* dip coating, spin coating, doctor blade coating) had a thickness limit of ~1 μm and could not be used to conformably coat high aspect ratio structures.[39] In an early work by Foong *et al.*, TiO_2 was deposited on a porous anodic aluminum oxide (AAO) substrate to obtain an array of well-aligned nanotubes.[40] The TiO_2 nanotubes were obtained by exposing the AAO substrates to a solution of titanium(IV) isopropoxide (TTIP) in toluene and an ethanolic solution of 10% deionized (DI) water in a sequential fashion with in between rinsing and drying steps (Fig. 2). An almost constant growth per cycle (GPC) of 2.4 Å was determined by following the frequency decrease of a QCM caused by the mass uptake of the solid film. Interestingly, the observed growth rate was comparable to the gas phase version of the process,[41,42] and the resulting films were smooth and conformal to the nanometer scale. In addition, the as-deposited TiO_2 nanotubes displayed a certain degree of crystallinity as demonstrated by high-resolution transmission electron microscopy (TEM) images and their corresponding selected area diffraction (SAD) patterns. The processing of crystalline materials at low temperatures is highly desired for the fabrication of flexible devices on temperature-sensitive plastic substrates[43] and microelectromechanical systems (MEMS).[44]

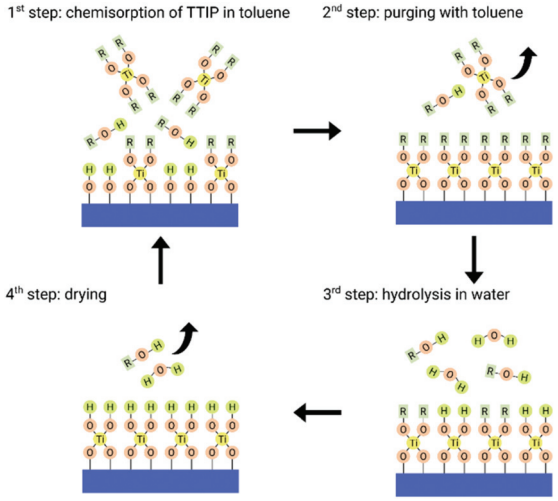

Fig. 2 Schematics of TiO_2 LALD based on the SSG approach. Adapted with permission from ref. 40. Copyright 2010, John Wiley & Sons.

The doping of materials has also been achieved by LALD based on sol–gel reactions as demonstrated by Shen *et al.*[45] In their work, TiO_2 was doped with different vanadium mole ratios (5% and 10%) to improve its photocatalytic activity. In contrast with other doping methods such as impregnation and co-precipitation, where the substitution of the dopant may take place only on the surface and dopant oxide aggregates might be formed, the LALD process ensures the incorporation of the dopant at the atomic level. The photocatalytic performance of undoped and vanadium(V)-doped TiO_2 was evaluated by the photodegradation of methylene blue (MB) aqueous solutions under visible light illumination. The degradation rate of MB obtained with the 5% and 10% vanadium-doped samples was four and five times higher than that of undoped TiO_2. The authors attribute this higher degradation rate to the optical absorption shift from 355 nm (undoped TiO_2) to 410 nm (V-doped TiO_2) and to the suppression of electron–hole recombination centers.

Although LALD based on the SSG approach has been successfully used to produce metal oxide films, the methodology involves a drying step in between the cycles and requires fresh solutions after certain deposition cycles that make the overall process tedious and difficult to automate. To overcome these issues, sol–gel processes that do not involve the use of water have been proposed.[47–49] These non-hydrolytic methods are based on reactions between a metal or silicon halide and a metal or silicon alkoxide under anhydrous conditions to generate the corresponding metal oxides and volatile alkyl halides. Paradoxically, the literature reports of metal–oxide deposition *via* non-hydrolytic reactions exist only for gas-phase[50,51] ALD and remain to be adapted for LALD.

Water is one of the most used oxygen sources for the deposition of metal oxides in gas-phase ALD as its reaction with adsorbed surface molecular species gives way to the generation of surface –OH groups at modest temperatures.[52,53] Subsequently, these –OH groups react with the metal precursor to form M–O–M bonds and, after several cycles, a metal oxide thin film is obtained. Thus, so far, the majority of LALD reports that are based on hydrolytic reactions have been adapted from well-known gas-phase ALD chemistries. Nevertheless, it is important to remember that ALD reactions occurring in the gas phase have themselves been developed from solution-based inorganic chemistry and thus, some similarities can be expected.[54]

Following this principle, Alam *et al.* developed an automated LALD process for the deposition of TiO_2 and ZrO_2 films on silica fibers.[55] Contrary to the SSG approach, the whole process occurred under an inert atmosphere in the liquid phase and included, for the first time, a purging step with anhydrous ethanol to remove unreacted precursors and reaction byproducts. The as-deposited films were annealed at 700 °C for 5 h and used as a platform for studying the hydrogen (H_2) production by radiolysis of water absorbed on solid substrates. A strong decrease in H_2 production was observed as the TiO_2 film thickness increased. However, the production of H_2 was amplified in the case of ZrO_2 films.

Similarly, Wu *et al.* introduced a microfluidic-based LALD process for the deposition of TiO_2, MgO, and SiO_2.[46] A microfluidic chip made out of Teflon was used as a reaction chamber for the deposition of thin films on planar substrates, whereas a stainless steel one was used for coating high-surface-area porous substrates. The authors demonstrated the self-saturating characteristic of the LALD chemistry by following the growth rate of TiO_2 at different precursor pulse durations (Fig. 3d). However, the as-obtained TiO_2 films were rough and amorphous (Fig. 3b), suggesting a poorer quality than some of the films obtained with gas-phase ALD.[57] In addition, MgO was deposited using ethylmagnesium chloride (EtMgCl) to demonstrate the wider availability of precursors in the liquid phase as Grignard reagents have failed to be implemented in gas-phase ALD.

In a different approach, Le Monnier *et al.* developed a stoichiometrically-limited LALD process to deposit aluminum oxide (Al_2O_3) on high-surface-area substrates without the need for excess precursors or purging with pure solvent.[56] Their methodology relies on determining by titration the exact quantities of trimethyl aluminum (TMA) and H_2O needed to fully react with a silica powder substrate to obtain a monolayer of Al_2O_3 (Fig. 4). By taking gas samples from the reactor, the methane released after each addition of TMA and H_2O could be quantified, and thus, the saturation point of both precursors could be established. The applicability of the method for catalysis was demonstrated by comparing the dispersion of coated and uncoated palladium nanoparticles supported on silica after continuous cycles of thermal treatment. The accessibility for palladium sites remained unaffected on the coated palladium catalyst and decreased for the uncoated ones due to sintering. In addition, aluminum phosphate ($AlPO_4$) was deposited from TMA and phosphoric acid to demonstrate the applicability of the process for depositing materials that are difficult to prepare by conventional gas-phase ALD given the low vapor pressure of several phosphate precursors.

These examples further demonstrate the feasibility of applying LALD to implement the well-known hydrolytic gas-phase ALD reactions in the liquid phase and, moreover, introduce reactions that cannot be performed in the gas phase.

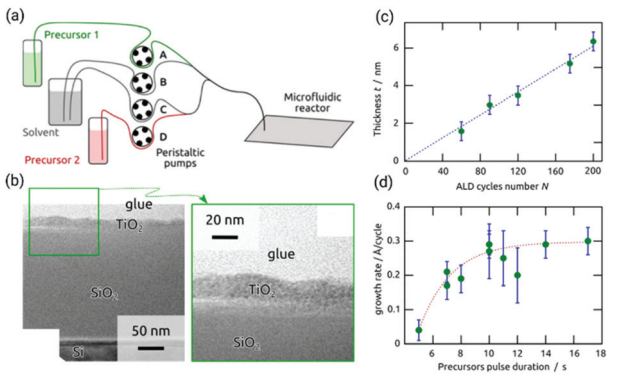

Fig. 3 (a) Schematics of a microfluidic-based LALD setup. (b) TiO_2 film deposited by a microfluidic-based LALD system on a Si wafer with 200 nm of thermal SiO_2. (c) Proportional growth of a TiO_2 film as the number cycles increases and (d) saturation of the growth at a certain precursor dosage for a microfluidic-based LALD process. Adapted with permission from ref. 46. Copyright 2015, American Chemical Society.

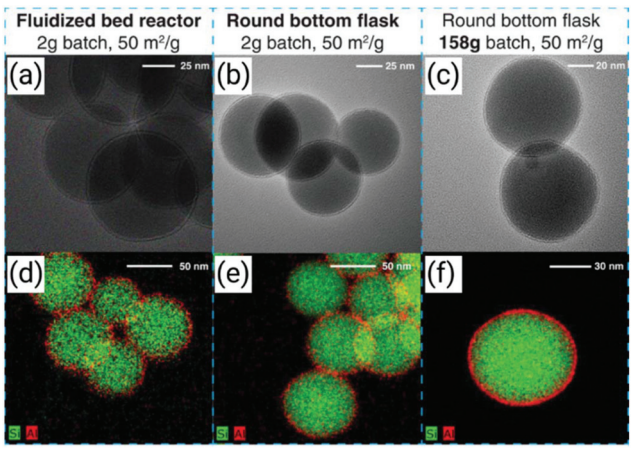

Fig. 4 (a–c) Bright-field transmission electron microscopy (TEM) images of silica nanospheres coated with ten cycles of Al_2O_3 by using (a) a fluidized bed reactor ALD (2 g batch) and (b and c) a round bottom flask (2 g batch, and 158 g batch, respectively). (d and e) Scanning transmission electron microscopy (STEM)-energy dispersive X-ray (EDX) elemental mapping of Si and Al of silica nanospheres coated with Al_2O_3 by using (d) a fluidized bed reactor ALD (2 g batch) and (e and f) a round bottom flask (2 g batch, and 158 g batch, respectively) adapted with permission from ref. 56. Copyright 2019, John Wiley & Sons.

LALD based on non-conventional reaction strategies

Besides sol–gel chemistry and hydrolytic reactions, LALD approaches based on other mechanisms such as redox reactions and condensation/polymerization have been recently explored. For example, Zankowski *et al.* developed an elegant method for the deposition of manganese dioxide (MnO_2) that is driven by cyclic redox reactions and is referred to as redox layer deposition (RLD).[58] In their work, potassium permanganate ($KMnO_4$) was used as the manganese precursor while propargyl alcohol (PA) acted as the permanganate reducer. MnO_2 films were obtained by immersing Ni/TiN/Si wafers in glass vessels containing aqueous solutions of PA and $KMnO_4$ separated by a rinsing step with DI water. In addition, the suitability of the process for high aspect ratio structures was demonstrated by coating 3D Ni nanomesh substrates (Fig. 5a–d). An even distribution of MnO_2 could be observed after quantifying the Mn/Ni ratio along the entire thickness of the nanomesh (Fig. 5e). Conversely, only the top part of the Ni nanomesh was covered when traditional gas-phase ALD was performed.

A systematic study by cyclic voltammetry (CV) of the growth dynamics showed that the deposition followed an adsorption-driven growth that was affected by the equilibrium between MnO_2 deposition and a side reaction with PA and thus resulted in a large error of the estimated GPC. Nevertheless, after fitting the experimental data to a Lagergen-like kinetics equation, a GPC (1.2 ± 0.2 Å) was obtained. Although relatively small, this GPC was found to be higher than the one for gas-phase ALD (0.15–0.3 Å). Indeed, the low GPC frequently observed in gas-phase ALD systems for the deposition of MnO_2 is ascribed to the steric hindrance effects caused by bulky metal–organic precursors. In contrast, due to the small size of the PA molecules and the MnO_4^- ions, MnO_2 deposition can take place more freely at the surface of a substrate and thus a higher GPC can be expected.

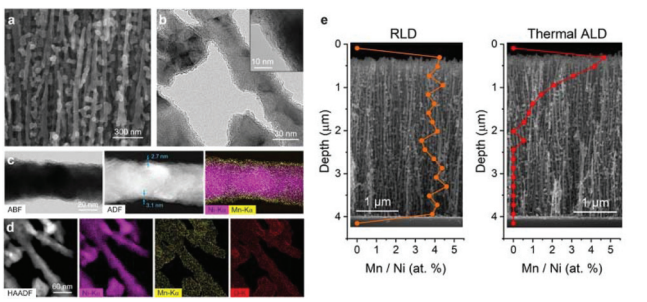

Fig. 5 (a) SEM image of the MnO_2-coated Ni nanomesh network. (b) TEM image of the Ni nanomesh network coated with 15 cycles of RLD. (c) Annular bright-field (ABF) and annular dark-field (ADF) STEM images of a single Ni nanowire coated with MnO_2 with their complementary EDX elemental mapping of Ni and Mn. (d) High-angle annular dark-field (HAADF) STEM image and complementary EDX elemental mapping of a Ni nanomesh cluster for Ni, Mn, and O. (e) EDX-scanning electron microscopy (SEM) picture of the Mn content along the breadth of the 3D Ni nanomesh covered by LALD (left) and gas-phase ALD (right). Adapted with permission from ref. 58. Copyright 2019, American Chemical Society.

Furthermore, to test the viability of the MnO_2-coated Ni nanomesh to be used as Li-ion electrodes, CV was performed in a solution of $LiClO_4$/propylene carbonate. Redox peaks corresponding to anodic and cathodic shoulders at 2.65 V and 3.6 V *vs.* Li^+/Li could be observed, while no visible peaks could be discerned for films obtained with gas-phase ALD. However, the MnO_2 films obtained with LALD had a lower electrochemical performance when compared to gas-phase ALD films obtained on flat substrates.[59]

Unlike crystalline MnO_2 thin films prepared by gas-phase ALD,[60,61] the films obtained by the LALD redox approach were amorphous with a few small crystalline regions. On that account, although it is known that the higher temperatures required for gas phase ALD together with the truly self-saturating behavior of the reactions improve the crystallinity of the synthesized materials, techniques based on heterogeneous nucleation processes can be employed in principle for the growth of crystalline films.

Toward that goal, Taniguchi *et al.* introduced an LALD approach based on the spin spray (SPS) technique for the deposition of hematite (α-Fe_2O_3) thin films.[62] In this method, precursor solutions of $FeCl_2$ and $NaNO_2$ were continuously sprayed on glass substrates mounted on a heated spinning stage at ambient pressure. The deposition mechanism followed the simultaneous adsorption of Fe^{2+} ions on the hydroxylated surface of the substrate and their subsequent oxidation to Fe^{3+} by the oxidizer to form O–Fe–O bonds. XRD patterns of the resulting material showed that only the α-Fe_2O_3 phase with a preferential growth along the (012) plane was present, while no undesired phases, such as $Fe(OH)_2$, $Fe(OH)_3$, FeOOH, Fe_3O_4, and γ-Fe_2O_3 could be detected. Furthermore, no XRD peaks could be observed for samples prepared with conventional aqueous precipitation processes involving $FeCl_3$ as the Fe^{3+} source and CH_3COONa as the pH adjuster (Fig. 6a). The crystalline α-Fe_2O_3 thin films displayed desirable ALD traits such as uniform thickness, high transparency, and strong adhesion to the substrate (Fig. 6b and c). Remarkably, when compared to the relatively high temperature needed to deposit hematite with gas-phase ALD,[63] this high degree of crystallinity and ALD features were obtained at a low temperature of 95 °C, which makes the technique appealing for depositing on temperature-sensitive substrates such as polyethylene terephthalate (PET).

Being closely related to ALD, molecular layer deposition (MLD) is another important gas-phase technique that is also based on surface sequential, self-limiting reactions.[64,65] However, in MLD, at least one of the reagents is purely organic and is deposited at each of the precursor pulsing steps. A prominent approach aiming to expand LALD for the deposition of purely organic and hybrid organic–inorganic films based on MLD has been recently proposed by Fichtner *et al.*[66] After protecting the amine group of a heterobifunctional monomer (*para*-aminobenzoic acid [*p*-ABA]) with *tert*-butyloxycarbonyl (Boc), and enhancing the reactivity of its acyl group with (3-dimethlyaminopropyl)carbodiimide (EDC), the resulting monomer (Boc-*p*-ABA-EDC) can react with the surface of a Si

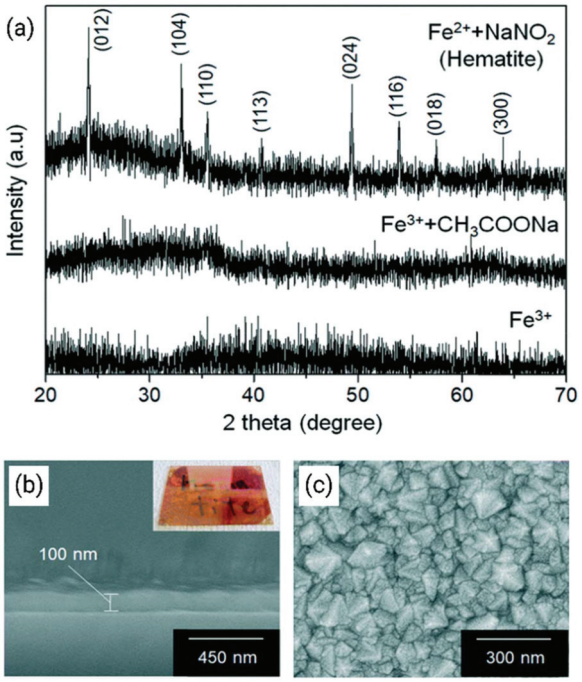

Fig. 6 (a) XRD patterns of the films grown by LALD based on SPS using $FeCl_2/NaNO_2$, $FeCl_3/CH_3COONa$, and $FeCl_3$ precursors. (b) Cross-sectional and (c) top view SEM images of the α-Fe_2O_3 films deposited by LALD based on SPS. The inset in (b) shows a photograph of the film. Adapted with permission from ref. 62. Copyright 2019, Royal Society of Chemistry.

substrate and, subsequently, with trifluoroacetic acid (TFA) to deposit an aromatic polyamide (poly-*p*-ABA) thin film (Fig. 7a and b).

After varying the duration of the precursor pulses, the self-limiting behavior of the reactions was demonstrated by ellipsometry and a constant GPC of 1 (±0.1) Å was observed. In addition, after analyzing a sample of Boc-*p*-ABA monomer treated with a stoichiometric amount TFA and the poly-*p*-ABA thin film by mass spectrometry, the covalent polymerization character of the film was demonstrated by the absence of a signal corresponding to the Boc-*p*-ABA monomer on the thin film spectrum.

These examples reinforce the remarkable potential of LALD for the deposition of thin films by being adaptable to a diverse range of surface chemistries, in which different types of equipment configurations (*e.g.* laboratory glassware, microfluidic reactors) can be used.

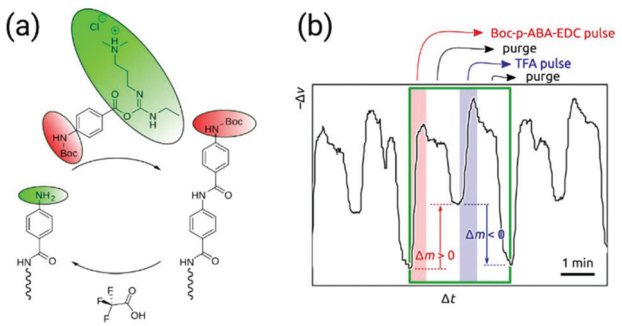

Fig. 7 (a) Reaction scheme for the deposition of poly-*p*-ABA. The heterobifunctional precursor (Boc-*p*-ABA-EDC) reacts with the amino group of surface-attached *p*-ABA. Next, the Boc-protected surface is reacted with TFA to render the surface active for a new cycle. (b) Change of QCM oscillator frequency (Δf) as a function of time of multiple deposition cycles. A green frame is superimposed to delimit one deposition cycle. The precursor pulses are highlighted in red (Boc-*p*-ABA-EDC) and blue (TFA). Adapted with permission from ref. 66. Copyright 2017, IOP Publishing.

Conclusions and outlook

Liquid phase atomic layer deposition is a valuable technique that has been approached from different angles over the years but has just recently begun to be explored and applied in the fabrication of high quality materials as demonstrated by the summary of works discussed in this short article. Table 1 includes a list of all the reported LALD approaches with a description of the materials, precursors, type of reaction, substrates, grow rates per cycle, and automatization (if applicable). The high precision thickness control, excellent conformality, and possibility of being automated in a simple and inexpensive way have enabled its differentiation from similar thin film deposition techniques performed in the liquid phase.[68] Moreover, in contrast to gas-phase ALD in which precursors must meet requirements such as having an appropriate vapor pressure and good thermal stability,[69] LALD can be performed with a broader diversity of well-known cheap reagents already used in solution chemistry. Herein, we have called attention to the current strengths of LALD for the fabrication of thin-film materials while, at the same time, hinted towards improvements that can allow it to become a mature technology. For instance, the lack of a general approach involving an easy-to-reproduce setup built from materials that can be compatible with the overall harsh solvents and anhydrous conditions required to perform the deposition is something that needs to be addressed. Moreover, as most of the approaches discussed here are performed using bulky lab glassware and extensive manual labor, a need of simple automated systems is evident to compete with traditional gas-phase ALD systems. On this issue, 3D-printed microfluidic setups could be implemented to LALD as they can be easily customized by using computer-aided software (CAD)[70] and can be built from solvent-compatible materials (*e.g.* polytetrafluoroethylene [PTFE],[71] 1*H*,1*H*,6*H*,6*H*-perfluoro-1,6-hexyl diacrylate [PFHDA][72]). The versatility offered by 3D printing has indeed already been exploited to fabricate custom SALD heads.[73,74] Furthermore, the challenges associated with the overall slow growth rate and poor control over the morphology, surface roughness, and density of the films need to be addressed as the overall quality of the films is impacted by these properties.[75] For example, MnO_2 films deposited by LALD[58] have a lower electrochemical performance when compared to films deposited by gas-phase ALD.[59] To solve these pro-

Table 1 List of LALD approaches

Reaction strategy	Material	Precursor A	Precursor B	Solvent	Substrate	Growth rate (cycle^{-1})	Automated	Ref.
Hydrolysis	TiO_2	$Ti(OBu)_4$	H_2O	$Ti(OBu)_4$: EtOH H_2O : –	SiO_2 fiber filter	—	Yes	55
Hydrolysis	ZrO_2	$Zr(O^nPr)_4$	H_2O	$Zr(O^nPr)_4$: EtOH H_2O : EtOH	SiO_2 fiber filter	—	Yes	55
Sol–gel (SSG)	TiO_2	$Ti(O^iPr)_4$	H_2O	$Ti(O^iPr)_4$: toluene H_2O : EtOH	Si, AAO	2.4 Å	No	40
Sol–gel (SSG)	V-Doped TiO_2	$Ti(O^iPr)_4$	$VO(O^iPr)_3$	$Ti(O^iPr)_4$: toluene : EtOH $VO(O^iPr)_3$: toluene : EtOH	Si	4.0 Å	No	45
Hydrolysis	TiO_2	$Ti(O^iPr)_4$	H_2O	$Ti(O^iPr)_4$: Et_2O H_2O : Et_2O	Si (100)/SiO_2	0.3 Å	Yes	46
Hydrolysis	SiO_2	$HSiCl_3$	H_2O	$HSiCl_3$: Et_2O H_2O : Et_2O	Si (100)/SiO_2, AAO	1.7 Å	Yes	46
Hydrolysis (Grignard reagent)	MgO	EtMgCl	H_2O	EtMgCl : Et_2O H_2O : Et_2O	Si (100)/SiO_2	1.0 Å	Yes	46
Polymerization	Poly-*p*-ABA	Boc-*p*-ABA-EDC	TFA	Boc-*p*-ABA-EDC : MeCN TFA : MeCN	Si (100)/SiO_2	1.0 Å	Yes	66
Redox	MnO_2	$KMnO_4$	PA	$KMnO_4$: H_2O PA : H_2O	Ni/TiN/Si, 3D Ni nanomesh/Al/TiN/Si	1.2 Å	No	58
Hydrolysis	Al_2O_3	TMA	H_2O	TMA : $nBuO_2$ H_2O : dioxane	SiO_2	4.5 atom nm^{-2}	No	56
Precipitation	$AlPO_4$	TMA	H_3PO_4	TMA : DBE H_3PO_4 : DBE	SiO_2	—	No	56
Precipitation	ZnS	DEZ	H_2S	DEZ : heptane : DBE H_2S : THF : DBE	SiO_2	—	No	56
Redox	α-Fe_2O_3	$FeCl_2$	$NaNO_2$	$FeCl_2$: H_2O $NaNO_2$: H_2O	Glass	6.3 nm	Yes	62
Redox	MnO_2	$KMnO_4$	PA	$KMnO_4$: H_2O PA : H_2O	3D Ni nanomesh	1.7 Å	No	67

blems, post-annealing treatments could help improve the overall crystallinity of the films, while adhesion layers could be introduced to control their growth mode and morphology.[76] In summary, despite the significant advances achieved in LALD in the past few years, there are still exciting challenges and opportunities that need to be satisfied to bring the technology to a wider audience and pave its way for greater practical applications.

Conflicts of interest

There are no conflicts to declare.

Acknowledgements

This work was partially supported by the Fondation Nanosciences (Université Grenoble Alpes, France) through the M-O-Films project. J. P.-L. acknowledges funding by the European Research Council Starting Grant microCrysFact (ERC-2015-STG No. 677020) and the Swiss National Science Foundation (project no. 200021_181988). J. P.-L. and D. M.-R. acknowledge support from the European Union's Horizon 2020 FETOPEN-1-2016-2017 research and innovation program under Grant Agreement 801464.

Notes and references

1 J. E. Greene, *J. Vac. Sci. Technol., A*, 2017, **35**, 05C204.
2 L. Hoffmann, K. O. Brinkmann, J. Malerczyk, D. Rogalla, T. Becker, D. Theirich, I. Shutsko, P. Görrn and T. Riedl, *ACS Appl. Mater. Interfaces*, 2018, **10**, 6006–6013.
3 D. P. Monaghan, D. G. Teer, P. A. Logan, K. C. Laing, R. I. Bates and R. D. Arnell, *Surf. Coat. Technol.*, 1993, **60**, 592–596.
4 M. Kamalisarvestani, R. Saidur, S. Mekhilef and F. S. Javadi, *Renewable Sustainable Energy Rev.*, 2013, **26**, 353–364.
5 A. Kriele, O. A. Williams, M. Wolfer, D. Brink, W. Müller-Sebert and C. E. Nebel, *Appl. Phys. Lett.*, 2009, **95**, 031905.
6 C.-H. Lambert, S. Mangin, B. S. D. Ch. S. Varaprasad, Y. K. Takahashi, M. Hehn, M. Cinchetti, G. Malinowski, K. Hono, Y. Fainman, M. Aeschlimann and E. E. Fullerton, *Science*, 2014, **345**, 1337–1340.
7 J. E. Crowell, *J. Vac. Sci. Technol., A*, 2003, **21**, S88–S95.
8 M. Benelmekki and A. Erbe, in *Frontiers of Nanoscience*, Elsevier Ltd, 2019, vol. 14, pp. 1–34.
9 J. E. Greene, *Appl. Phys. Rev.*, 2014, **1**, 041302.
10 J. Schmitz, *Surf. Coat. Technol.*, 2018, **343**, 83–88.
11 Z. H. Barber, *J. Mater. Chem.*, 2006, **16**, 334–344.
12 A. Yanguas-Gil, *Growth and Transport in Nanostructured Materials*, Springer International Publishing, 2017.

13 C. Crivello, S. Sevim, O. Graniel, C. Franco, S. Pané, J. Puigmartí-Luis and D. Muñoz-Rojas, *Mater. Horiz.*, 2021, **8**, 168–178.
14 S. M. George, *Chem. Rev.*, 2010, **110**, 111–131.
15 O. Graniel, M. Weber, S. Balme, P. Miele and M. Bechelany, *Biosens. Bioelectron.*, 2018, **122**, 147–159.
16 D. Muñoz-Rojas and J. MacManus-Driscoll, *Mater. Horiz.*, 2014, **1**, 314–320.
17 F. Zaera, *J. Phys. Chem. Lett.*, 2012, **3**, 1301–1309.
18 A. Devi, *Coord. Chem. Rev.*, 2013, **257**, 3332–3384.
19 D. Muñoz-Rojas, T. Maindron, A. Esteve, F. Piallat, J. C. S. Kools and J.-M. Decams, *Mater. Today Chem.*, 2019, **12**, 96–120.
20 J. A. Switzer and G. Hodes, *MRS Bull.*, 2010, **35**, 743–750.
21 Y. F. Nicolau, *Appl. Surf. Sci.*, 1985, **22–23**, 1061–1074.
22 H. M. Pathan and C. D. Lokhande, *Bull. Mater. Sci.*, 2004, **27**, 85–111.
23 R. Parize, T. Cossuet, E. Appert, O. Chaix-Pluchery, H. Roussel, L. Rapenne and V. Consonni, *CrystEngComm*, 2018, **20**, 4455–4462.
24 H. Lee, M. Wang, P. Chen, D. R. Gamelin, S. M. Zakeeruddin, M. Grätzel and M. K. Nazeeruddin, *Nano Lett.*, 2009, **9**, 4221–4227.
25 N. S. Mohamed Mustakim, C. A. Ubani, S. Sepeai, N. Ahmad Ludin, M. A. Mat Teridi and M. A. Ibrahim, *Sol. Energy*, 2018, **163**, 256–270.
26 M. Jana, S. Saha, P. Samanta, N. C. Murmu, N. H. Kim, T. Kuila and J. H. Lee, *J. Power Sources*, 2017, **340**, 380–392.
27 D. P. Dubal, G. S. Gund, C. D. Lokhande and R. Holze, *ACS Appl. Mater. Interfaces*, 2013, **5**, 2446–2454.
28 H. Li, Z. Xia, J. Chen, L. Lei and J. Xing, *Appl. Catal., B*, 2015, **168–169**, 105–113.
29 Y. Zhu, Y. Wang, Z. Chen, L. Qin, L. Yang, L. Zhu, P. Tang, T. Gao, Y. Huang, Z. Sha and G. Tang, *Appl. Catal., A*, 2015, **498**, 159–166.
30 B. Çakıroğlu and M. Özacar, *Biosens. Bioelectron.*, 2019, **141**, 111385.
31 J. Gong, X. Wang, X. Li and K. Wang, *Biosens. Bioelectron.*, 2012, **38**, 43–49.
32 S. Lindroos and M. Leskelä, in *Solution Processing of Inorganic Materials*, ed. D. B. Mitzi, John Wiley & Sons, Inc., Hoboken, NJ, USA, 2009, pp. 239–282.
33 B. W. Gregory and J. L. Stickney, *J. Electroanal. Chem. Interfacial Electrochem.*, 1991, **300**, 543–561.
34 W. Zhu, X. Liu, H. Liu, D. Tong, J. Yang and J. Peng, *J. Am. Chem. Soc.*, 2010, **132**, 12619–12626.
35 J. L. Stickney, in *Electroanalytical Chemistry: A Series of Advances*, ed. I. Rubinstein, CRC Press, Boca Raton, 1st edn, 1999, pp. 75–209.
36 J. L. Stickney, *Electrochem. Soc. Interface*, 2011, **20**, 28–30.
37 I. Ichinose, H. Senzu and T. Kunitake, *Chem. Lett.*, 1996, **25**, 831–832.
38 Y. Aoki and T. Kunitake, *Adv. Mater.*, 2004, **16**, 118–123.
39 I. Ichinose, H. Senzu and T. Kunitake, *Chem. Mater.*, 1997, **9**, 1296–1298.
40 T. R. B. Foong, Y. Shen, X. Hu and A. Sellinger, *Adv. Funct. Mater.*, 2010, **20**, 1390–1396.
41 J. Aarik, A. Aidla, T. Uustare, M. Ritala and M. Leskelä, *Appl. Surf. Sci.*, 2000, **161**, 385–395.
42 M. Aghaee, P. S. Maydannik, P. Johansson, J. Kuusipalo, M. Creatore, T. Homola and D. C. Cameron, *J. Vac. Sci. Technol., A*, 2015, **33**, 041512.
43 A. K. Chandiran, A. Yella, M. Stefik, L.-P. Heiniger, P. Comte, M. K. Nazeeruddin and M. Grätzel, *ACS Appl. Mater. Interfaces*, 2013, **5**, 3487–3493.
44 Y. Huang, G. Pandraud and P. M. Sarro, *J. Vac. Sci. Technol., A*, 2013, **31**, 01A148.
45 Y. Shen, T. R. B. Foong and X. Hu, *Appl. Catal., A*, 2011, **409–410**, 87–90.
46 Y. Wu, D. Döhler, M. Barr, E. Oks, M. Wolf, L. Santinacci and J. Bachmann, *Nano Lett.*, 2015, **15**, 6379–6385.
47 R. Corriu, D. Leclercq, P. Lefevre, P. H. Mutin and A. Vioux, *Chem. Mater.*, 1992, **4**, 961–963.
48 A. Vioux, *Chem. Mater.*, 1997, **9**, 2292–2299.
49 W. Yan, S. M. Mahurin, S. H. Overbury and S. Dai, *Chem. Mater.*, 2005, **17**, 1923–1925.
50 M. Ritala, K. Kukli, A. Rahtu, P. I. Räisänen, M. Leskelä, T. Sajavaara and J. Keinonen, *Science*, 2000, **288**, 319–321.
51 E. Rauwel, G. Clavel, M.-G. Willinger, P. Rauwel and N. Pinna, *Angew. Chem., Int. Ed.*, 2008, **47**, 3592–3595.
52 M. Leskelä and M. Ritala, *Thin Solid Films*, 2002, **409**, 138–146.
53 G. Clavel, E. Rauwel, M. G. Willinger and N. Pinna, *J. Mater. Chem.*, 2009, **19**, 454–462.
54 S. T. Barry, A. V. Teplyakov and F. Zaera, *Acc. Chem. Res.*, 2018, **51**, 800–809.
55 M. Alam, F. Miserque, M. Taguchi, L. Boulanger and J. P. Renault, *J. Mater. Chem.*, 2009, **19**, 4261.
56 B. P. Le Monnier, F. Wells, F. Talebkeikhah and J. S. Luterbacher, *Adv. Mater.*, 2019, **31**, 1904276.
57 S. K. Song, H. Saare and G. N. Parsons, *Chem. Mater.*, 2019, **31**, 4793–4804.
58 S. P. Zankowski, L. van Hoecke, F. Mattelaer, M. de Raedt, O. Richard, C. Detavernier and P. M. Vereecken, *Chem. Mater.*, 2019, **31**, 4805–4816.
59 F. Mattelaer, P. M. Vereecken, J. Dendooven and C. Detavernier, *Chem. Mater.*, 2015, **27**, 3628–3635.
60 O. Nilsen, S. Foss, H. Fjellvåg and A. Kjekshus, *Thin Solid Films*, 2004, **468**, 65–74.
61 S. Foss, O. Nilsen, A. Olsen and J. Taftø, *Philos. Mag.*, 2005, **85**, 2689–2705.
62 A. Taniguchi, T. Taniguchi, H. Wagata, K. Katsumata, K. Okada and N. Matsushita, *CrystEngComm*, 2019, **21**, 4184–4191.
63 L. Steier, J. Luo, M. Schreier, M. T. Mayer, T. Sajavaara and M. Grätzel, *ACS Nano*, 2015, **9**, 11775–11783.
64 S. M. George, A. A. Dameron and B. Yoon, *Acc. Chem. Res.*, 2009, **42**, 498–508.
65 P. Sundberg and M. Karppinen, *Beilstein J. Nanotechnol.*, 2014, **5**, 1104–1136.
66 J. Fichtner, Y. Wu, J. Hitzenberger, T. Drewello and J. Bachmann, *ECS Trans.*, 2017, **80**, 63–73.

67 Y. Kee, B. Put, F. Bardé and P. M. Vereecken, *J. Electrochem. Soc.*, 2020, **167**, 020507.
68 I. Bretos, S. Diodati, R. Jiménez, F. Tajoli, J. Ricote, G. Bragaggia, M. Franca, M. L. Calzada and S. Gross, *Chem. – Eur. J.*, 2020, **26**, 9157–9179.
69 R. H. J. Vervuurt, W. M. M. (Erwin) Kessels and A. A. Bol, *Adv. Mater. Interfaces*, 2017, **4**, 1700232.
70 A. K. Au, W. Huynh, L. F. Horowitz and A. Folch, *Angew. Chem., Int. Ed.*, 2016, **55**, 3862–3881.
71 Y. Zhang, M.-J. Yin, X. Ouyang, A. P. Zhang and H.-Y. Tam, *Appl. Mater. Today*, 2020, **19**, 100580.
72 M. Männel, N. Hauck and J. Thiele, in *Microfluidics, BioMEMS, and Medical Microsystems XVIII*, ed. B. L. Gray and H. Becker, SPIE, 2020, vol. 11235, p. 17.
73 C. A. M. Huerta, V. H. Nguyen, A. Sekkat, C. Crivello, F. Toldra-Reig, P. B. Veiga, S. Quessada, C. Jimenez and D. Muñoz-Rojas, *Adv. Mater. Technol.*, 2020, 2000657.
74 V. H. Nguyen, A. Sekkat, C. A. Masse de la Huerta, F. Zoubian, C. Crivello, J. Rubio-Zuazo, M. Jaffal, M. Bonvalot, C. Vallée, O. Aubry, H. Rabat, D. Hong and D. Muñoz-Rojas, *Chem. Mater.*, 2020, **32**, 5153–5161.
75 K. S. Brown, C. Saggese, B. P. Le Monnier, F. Héroguel and J. S. Luterbacher, *J. Phys. Chem. C*, 2018, **122**, 6713–6720.
76 V. M. Koch, M. K. S. Barr, P. Büttner, I. Mínguez-Bacho, D. Döhler, B. Winzer, E. Reinhardt, D. Segets and J. Bachmann, *J. Mater. Chem. A*, 2019, **7**, 25112–25119.